引用格式：BAO Xiaoyan, DENG Shuo, LV Haifei, et al. Ellipsometric Measurement of the Refractive Index of Monocrystalline Silicon in a Diamond Anvil Cell[J]. Acta Photonica Sinica, 2023, 52(11):1112001
鲍晓艳,邓硕,吕海飞,等.金刚石压砧内单晶硅高压折射率的椭偏测量[J].光子学报,2023,52(11):1112001

金刚石压砧内单晶硅高压折射率的椭偏测量

鲍晓艳,邓硕,吕海飞,黎敏
(武汉理工大学 理学院,武汉 430070)

摘　要:针对高压对顶砧入射角度受限、样品微小的特殊测量条件,设计原位椭偏测量系统,实现450～700 nm光谱范围的小角度椭偏测量。建立光学模型,获得2～9 GPa下单晶硅的折射率,发现单晶硅的折射率随压力增加而增大。与高压拉曼光谱的对比说明椭偏法原位监测材料光学性质变化的可能性。本文研究可为高压下材料的光学常数及其原位测量提供有益补充。

关键词:高压;椭偏;光学模型;折射率;单晶硅
中图分类号:O43　　**文献标识码**:A　　**doi**:10.3788/gzxb20235211.1112001

0　引言

压力可导致物质的晶格结构改变[1],进而引起包括电子能带结构在内的多种物理、化学、机械性质发生改变。但是很多物质的高压相在常压下无法保持,因此,高压原位(in situ)测量技术是理解高压下物质结构及其转变的关键手段。现有的高压加载技术中,金刚石对顶砧(Diamond Anvil Cell,DAC)通过施加在面积极小但硬度极高的金刚石砧面上的压力产生极大的压强,是目前唯一能够实现1 000 GPa以上压力的静高压装置[2]。DAC技术在不断发展过程中,通过改善切割倒角、改进垫片材料和引入传压介质等,不断提升实验极限压力,极大地促进了高压实验技术的发展。同时,因金刚石从远红外至γ射线电磁波谱区都具有良好的透光性,因此,具有易与光学测试技术结合的先天优势。目前,拉曼光谱[3-7]、同步X光辐射[8-10]、紫外/可见光/红外光谱[11-15]等商用仪器均已被用于原位探测高压下材料性质的变化。然而,以上基于特征光谱吸收的高压原位测量方法均无法获取材料的光学常数,或者说更准确地描述材料性质的变化过程。椭偏测量技术作为一种代表性的光学测试手段,可准确测量薄膜的介电常数(及厚度)。但是,受到DAC小入射孔径和小样品尺寸(百微米量级)的结构限制,商业椭偏仪无法实现直接测量。而由于高压环境的特殊性,国际上针对DAC结构的椭偏测量研究偏少。NISSIM N课题组在2009年和2011年分别报道了采用单一波长椭偏法测试铁的光学常数的结果[16,17],观察到了铁的相变。国内华中科技大学在现有椭偏仪上增加会聚透镜,并且对DAC装置进行扩大测量角度的改造加工,得到铁在320～1 690 nm波段的椭偏参数和10 GPa内拟合的光学常数[18]。因此,需要一种面向DAC结构设计的椭偏测量装置以实现高压下材料光学常数的原位监测。

单晶硅作为应用最广泛的半导体材料,是现代集成电路行业和微光学加工中最常见基底材料[19,20],其常压下的光学性质已非常清晰。然而,硅晶体在高压加载下会发生一系列相变并金属化,其物理性质也会随之而变化,其中的过程目前并不清楚,缺乏物性常数和有效的监测手段。而光学常数恰好可用以记录此一系列变化过程。获取单晶硅在不同压力加载下的光学常数信息能够进一步推算其电导率等电学参数。同时,硅作为常用的光学衬底材料,其压力加载下光学常数的变化规律也是研究材料在高压下性质的基础。本文通过自主设计的斯托克斯椭偏测量系统,实现适用于常规DAC装置的小角度多波长椭偏参数测量,结合光学建模,获取不同压力下单晶硅的光学常数。本文采用的椭偏法与高压加载技术相结合的测量方法,

基金项目:国家自然科学基金(Nos. 11974266, 62075174)
第一作者:鲍晓艳,249541@whut.edu.cn
通讯作者:黎敏,Email:minli@whut.edu.cn
收稿日期:2023-05-06;**录用日期**:2023-06-25

可以作为获取高压加载下物质光电性质的有力工具。

1 高压椭偏法原理

1.1 椭偏测量原理

偏振测量利用光束经过样品前后偏振特性的改变获取样品折射率、表面粗糙度等信息。如图1所示，通过分析入射光与出射光的偏振态，定义样品的椭偏参数ψ和Δ。

$$\rho=\frac{r_{\mathrm{p}}}{r_{\mathrm{s}}}=\tan\psi\mathrm{e}^{\mathrm{i}\Delta} \tag{1}$$

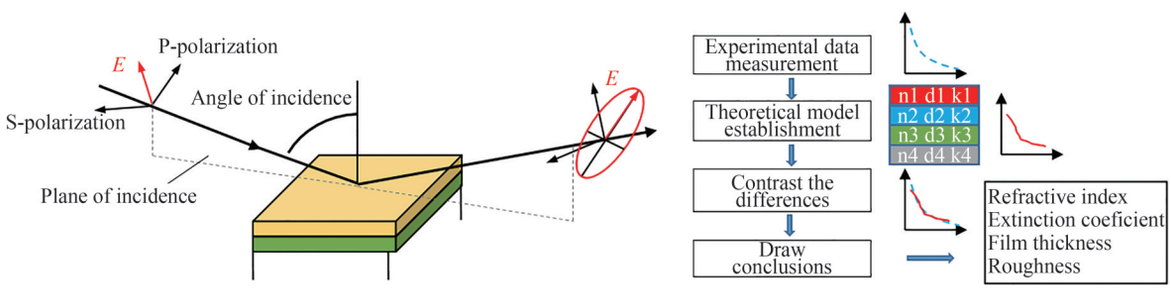

(a) Schematic diagram of polarized light reflection at the sample interface　　(b) Polarization measurement flow diagram

图1 偏振测量原理示意图

Fig. 1 Schematic diagram of polarization measurement principle

式中，ρ为p偏振光和s偏振光的反射系数r_{p}和r_{s}之比，Δ为p偏振分量和s偏振分量反射前后的相位差之差。实验中测量获取的椭偏参量ψ为角度值，此值与光线的入射角度、波长以及薄膜的光学常数和厚度等信息相关。椭偏测量分析流程如图1(b)所示。根据偏振矩阵运算表达式(2)，得到输出光的斯托克斯矢量S_{output}为

$$\begin{aligned}\boldsymbol{S}_{\mathrm{output}}&=\begin{bmatrix}S_0'\\S_1'\\S_2'\\S_3'\end{bmatrix}_{\mathrm{output}}=[\boldsymbol{M}]_{\mathrm{sample}}\hat{\boldsymbol{S}}_{\mathrm{input}}=\\&\begin{bmatrix}1&-\cos(2\psi)&0&0\\-\cos(2\psi)&1&0&0\\0&0&\sin(2\psi)\cos(\Delta)&\sin(2\psi)\sin(\Delta)\\0&0&-\sin(2\psi)\sin(\Delta)&\sin(2\psi)\cos(\Delta)\end{bmatrix}_{\mathrm{sample}}\begin{bmatrix}S_0\\S_1\\S_2\\S_3\end{bmatrix}_{\mathrm{input}}\end{aligned} \tag{2}$$

式中，$S_i(i=0,1,2,3)$依次表示总的入射光强、x分量和y分量的光强差、+45°和−45°偏振分量光强差、左旋和右旋圆偏振分量光强差。本文使用斯托克斯偏振测量仪得到样品反射光的椭偏参数。设置入射光具有特定偏振态$\boldsymbol{S}=(1,0,1,0)$，待测样品为各向同性。此时，测量得到反射光的斯托克斯矢量即可计算得到样品的椭偏参量ψ和Δ。

$$\begin{cases}\psi_{\mathrm{exp}}=\dfrac{1}{2}\arctan\left(\dfrac{\sqrt{S_2'^{\,2}+S_3'^{\,2}}}{-S_1'}\right)\\\Delta_{\mathrm{exp}}=\arctan\left(\dfrac{-S_3'}{S_2'}\right)\end{cases} \tag{3}$$

不同波长下，薄膜光学常数值与椭偏参数存在确定的对应关系，此为椭偏参数的数值拟合与光学常数反演问题。而通过椭偏参数拟合获得样品光学常数的关键在于DAC压腔内光学模型的建立，并通过式(4)的均方差函数评价光学常数拟合结果。

$$\mathrm{MSE}=\sqrt{\left(\psi_{\mathrm{exp}}-\psi_{\mathrm{model}}\right)^2+\left(\Delta_{\mathrm{exp}}-\Delta_{\mathrm{model}}\right)^2} \tag{4}$$

1.2 DAC高压光学模型的建立

高压椭偏测量不同于常规椭偏仪测量时的薄膜样品暴露于空气中，如图2所示的DAC结构与光路。待测样品所在高压区域为全密闭环境，入射光需经过数百微米尺度的金刚石窗口到达样品界面，因此需建立对应的光学模型（如图3所示）反演样品光学常数信息。

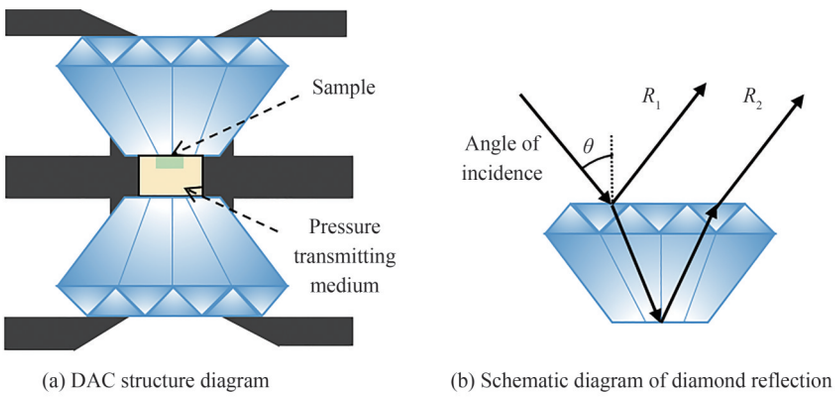

(a) DAC structure diagram　　(b) Schematic diagram of diamond reflection

图2　DAC结构及光路反射示意图

Fig. 2　DAC structure and optical path reflection diagram

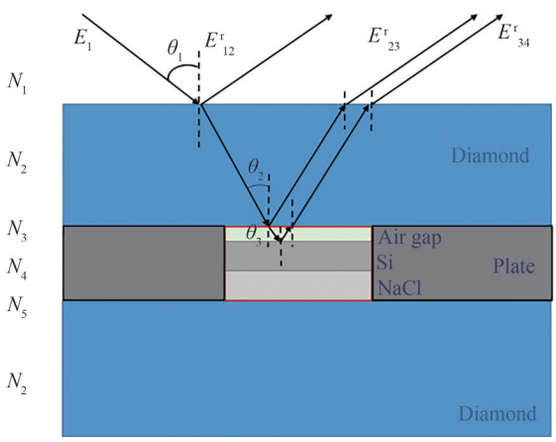

图3　适用DAC内的多层膜反射示意图

Fig. 3　Schematic diagram of multilayer reflection in DAC

因金刚石（N_2层）的厚度在毫米级，所以上部金刚石的上、下两表面（N_1N_2界面和N_2N_3界面）的反射光E^{r}_{12}和E^{r}_{23}并不相干，且可以将两束光分离，分别作为参考光和信号光进行分析。第一束（金刚石上表面N_1N_2界面）反射光E^{r}_{12}仅包含金刚石的折射率信息，第二束反射光E^{r}_{23}与E^{r}_{34}之和包含样品折射率信息。N_1N_2界面反射可依据菲涅尔公式推导得出；而在两层膜以上的模型中，由于膜层增多，反射和透射过程变复杂，采用矩阵理论分析更便捷。设用一个列矩阵表示准单色波的偏振特性，即

$$\begin{bmatrix} E^{\mathrm{p}} \\ E^{\mathrm{s}} \end{bmatrix} = \begin{bmatrix} E_0^{\mathrm{p}} \mathrm{e}^{\mathrm{i}\delta_1} \\ E_0^{\mathrm{s}} \mathrm{e}^{\mathrm{i}\delta_2} \end{bmatrix} \tag{5}$$

式中，E^{p}和E^{s}为直角坐标系中电场的p和s方向分量，E_0^{p}和E_0^{s}为电场分量的初始值，δ_1和δ_2为两分量的相位。光束在分界面上的反射或折射的过程可统一用式(6)和(7)表示，分别用i，r，t角标表示入射、反射与透射光

$$\begin{bmatrix} E_{\mathrm{r}}^{\mathrm{p}} \\ E_{\mathrm{r}}^{\mathrm{s}} \end{bmatrix} = \begin{bmatrix} r_{\mathrm{p}} & 0 \\ 0 & r_{\mathrm{s}} \end{bmatrix} \begin{bmatrix} E_{\mathrm{i}}^{\mathrm{p}} \\ E_{\mathrm{i}}^{\mathrm{p}} \end{bmatrix} = \boldsymbol{J}_{\mathrm{r}} \begin{bmatrix} E_{\mathrm{i}}^{\mathrm{p}} \\ E_{\mathrm{i}}^{\mathrm{p}} \end{bmatrix} \tag{6}$$

$$\begin{bmatrix} E_{\mathrm{t}}^{\mathrm{p}} \\ E_{\mathrm{t}}^{\mathrm{s}} \end{bmatrix} = \begin{bmatrix} t_{\mathrm{p}} & 0 \\ 0 & t_{\mathrm{s}} \end{bmatrix} \begin{bmatrix} E_{\mathrm{i}}^{\mathrm{p}} \\ E_{\mathrm{i}}^{\mathrm{p}} \end{bmatrix} = \boldsymbol{J}_{\mathrm{t}} \begin{bmatrix} E_{\mathrm{i}}^{\mathrm{p}} \\ E_{\mathrm{i}}^{\mathrm{p}} \end{bmatrix} \tag{7}$$

式中，r_{p}与r_{s}，t_{p}与t_{s}分别为菲涅尔公式求得的各界面反射与透射系数。光束通过厚度为d的各向同性薄膜的传输过程可表示为

$$\begin{bmatrix} E_{\text{output}}^{\text{p}} \\ E_{\text{output}}^{\text{s}} \end{bmatrix} = \begin{bmatrix} \text{e}^{-\text{j}2\pi nd/\lambda} & 0 \\ 0 & \text{e}^{-\text{j}2\pi nd/\lambda} \end{bmatrix} \begin{bmatrix} E_{\text{i}}^{\text{p}} \\ E_{\text{i}}^{\text{s}} \end{bmatrix} = \boldsymbol{M} \begin{bmatrix} E_{\text{i}}^{\text{p}} \\ E_{\text{i}}^{\text{s}} \end{bmatrix} \tag{8}$$

如图3所示的多层膜光束传输示意图，运用式(9)矩阵运算模拟光传输过程，其中矩阵$\boldsymbol{J}$表示界面透射、反射过程，分别用上标t，r表示，下标表示光界面传输，矩阵$\boldsymbol{M}$表示界面内传输过程，下标表示界面材料。高压界面反射光即R_2可由式(10)表示，并由式(11)求解得到椭偏参量理论值。

$$\begin{cases} \boldsymbol{E}_1 = \begin{bmatrix} E_{1\text{p}} \\ E_{1\text{s}} \end{bmatrix} \\ \boldsymbol{E}_{12}^{\text{r}} = \boldsymbol{J}_{12}^{\text{r}} \cdot \boldsymbol{E}_1 \\ \boldsymbol{E}_{23}^{\text{r}} = \boldsymbol{J}_{21}^{\text{t}} \cdot \boldsymbol{M}_2 \cdot \boldsymbol{J}_{23}^{\text{r}} \cdot \boldsymbol{M}_2 \cdot \boldsymbol{J}_{12}^{\text{t}} \cdot \boldsymbol{E}_1 \\ \boldsymbol{E}_{34}^{\text{r}} = \boldsymbol{J}_{21}^{\text{t}} \cdot \boldsymbol{M}_2 \cdot \boldsymbol{J}_{32}^{\text{t}} \cdot \boldsymbol{M}_3 \cdot \boldsymbol{J}_{34}^{\text{r}} \cdot \boldsymbol{M}_3 \cdot \boldsymbol{J}_{23}^{\text{t}} \cdot \boldsymbol{M}_2 \cdot \boldsymbol{J}_{12}^{\text{t}} \cdot \boldsymbol{E}_1 \end{cases} \tag{9}$$

$$\boldsymbol{E}_{\text{out}}^{\text{r}} = \boldsymbol{E}_{23}^{\text{r}} + \boldsymbol{E}_{34}^{\text{r}} = \begin{bmatrix} R_{\text{p}} & 0 \\ 0 & R_{\text{s}} \end{bmatrix} \begin{bmatrix} E_{\text{i}}^{\text{p}} \\ E_{\text{i}}^{\text{s}} \end{bmatrix} \tag{10}$$

$$\begin{cases} \tan\psi \cdot \text{e}^{\text{i}\Delta} = \dfrac{R_{\text{p}}}{R_{\text{s}}} \\ \psi_{\text{model}} = \arctan\left(\left| \dfrac{R_{\text{p}}}{R_{\text{s}}} \right| \right) \\ \Delta_{\text{model}} = \text{angle}\left(\dfrac{R_{\text{p}}}{R_{\text{s}}} \right) \end{cases} \tag{11}$$

另外，考虑金刚石表面存在不均匀粗糙层，对椭偏参数测量有一定影响。本文借助等效介质理论进一步分析。假设两种介质的不规则界面等效为一层有固定折射率和厚度的表面光滑薄膜，此薄膜对椭偏参数的影响与表面粗糙度等效。则最终光学模型为金刚石-等效膜层-样品三层膜结构。

为避免红宝石颗粒造成的界面不平整及易压碎硅片问题，本文通过金刚石拉曼进行压力标定[21]。本文采用拉曼光谱测试仪器测量金刚石表面拉曼峰，经过一阶求导后记录一阶最小峰值位置，并使用对应公式进行压力值换算，即

$$P(\text{GPa}) \cong A \frac{\Delta\omega}{\omega_0} \left[1 + \frac{1}{2}(B-1) \frac{\Delta\omega}{\omega_0} \right] \tag{12}$$

式中，$\Delta\omega$和ω_0分别代表频率偏移、常压下的频率，A，B为拟合参数值。

单晶硅的高压拉曼光谱测量实验采用加装50倍长焦镜头的拉曼光谱仪(SYC1227-4218F，HORIBA)，将波长532 nm的激发光聚焦于DAC内单晶硅表面，采样时长为3 s，记录采样光谱范围为300～800 cm^{-1}的数据并完成光强归一化处理，即获得对应压力下的单晶硅的拉曼光谱。

1.3 椭偏测量系统

图4是本文设计的高压椭偏测量系统图。从右到左依次为光源(Light source)、衰减滤波器(Filter)、光束调理系统，包括反射镜(Reflector)、格兰泰勒棱镜(Glan-Taylor polarizer)、会聚透镜(Focal lens)、DAC平台(电动微位移、旋转平台及相关旋转控制系统)和偏振测量仪(Polarization analyzer)。由于DAC的柱形结构，实验中的椭偏测量装置采用卧式，即入射和出射DAC的光平行于光学平台。超辐射白光激光器(SC-pro，安扬激光)发出的宽谱光经过声光滤波器(单波长输出带宽2～10 nm)输出；光束通过直角棱镜两次反射实现光路转折后，经格兰-泰勒棱镜输出特定方向线偏振光，再经由会聚透镜聚焦于压砧内的样品表面；可调焦成像系统CCD相机用来确认光斑聚焦位置。入射光分别经DAC的金刚石上下表面反射后，有两束反射光，在偏振测量仪(PAX1000VIS/M，Thorlabs)之前配置合适的狭缝，即可分别测量两束反射光的偏振态。

实验用高压椭偏测量系统中，光源的输出光斑大小约为2.1 μm，测量光谱范围为450～700 nm；伺服电机控制电动转台可实现0.04°的入射角度调节；紧凑型五轴微位移平台控制聚焦透镜，可实现x、y、z三轴3 mm量程和俯仰角±3.5°调节。

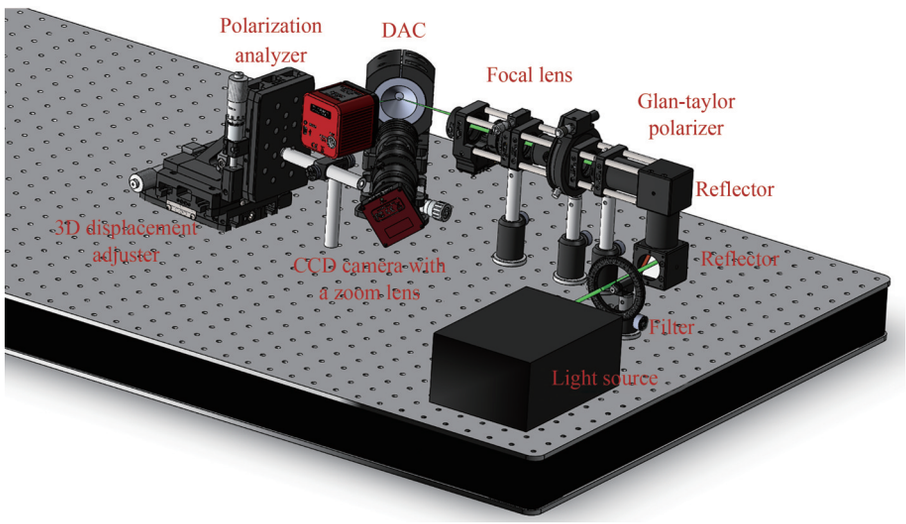

图4　原位高压椭偏测量系统示意图

Fig. 4　Schematic diagram of in situ high pressure ellipsometry measurement system

受DAC腔体尺寸的限制，测试样品厚度需控制在几十微米以下，而市售单晶硅片的厚度均大于100 μm。图5为单晶硅样品制备流程图。将单面抛光带25 nm氧化层的单晶硅片，用金刚石砂纸打磨至30 μm左右，使用激光切割为直径180 μm的圆片，清洗干燥后立即装填至压腔内，避免进一步氧化。使用铼片打孔在金刚石之间形成高压腔体，单晶硅抛光面紧挨金刚石一侧，并填充氯化钠粉末作为传压介质。

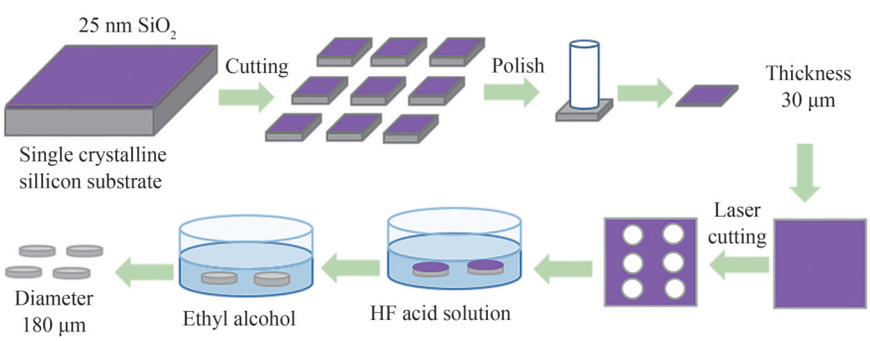

图5　单晶硅制备流程图

Fig. 5　Flowchart of monocrystalline silicon preparation

2　测量结果与讨论

在进行DAC高压椭偏测量前，首先使用椭偏测量系统对未加载压力（开放DAC）的单晶硅片进行椭偏测量，以验证实验系统的有效性。实验完成了入射角度分别为27°、30°、33°和40°的椭偏参数的测量（如图6所示）。然后，利用所建立的光学模型拟合得到单晶硅折射率，与椭偏仪VASE-V的测试结果及文献中Schinke测量结果[22]对比（如图7所示）。结果表明，在400～700 nm常压下单晶硅折射率测量结果与商用椭偏仪测量结果一致，这种一致性可证明本测量系统的可靠性。

高压下的椭偏测量包括金刚石上、下界面反射光的斯托克斯参量测量和使用金刚石拉曼光谱标定压力两个步骤。DAC未加压前，金刚石与单晶硅之间存在空气间隙，旋紧加压螺母的过程中，空气间隙减小，通

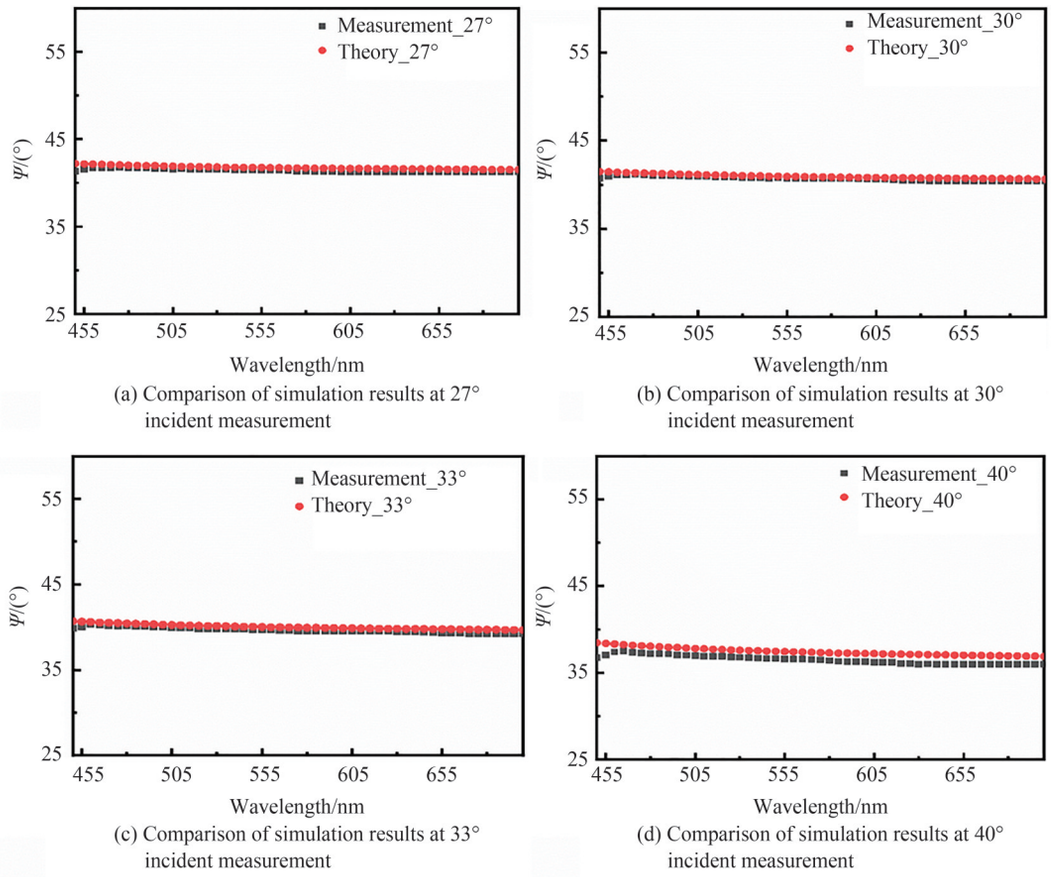

图 6 多角度斜入射单晶硅椭圆偏振参数测量仿真结果对比

Fig. 6 Comparison of simulation results of ellipsometry parameter measurement for monocrystalline silicon at multiple angles oblique incidence

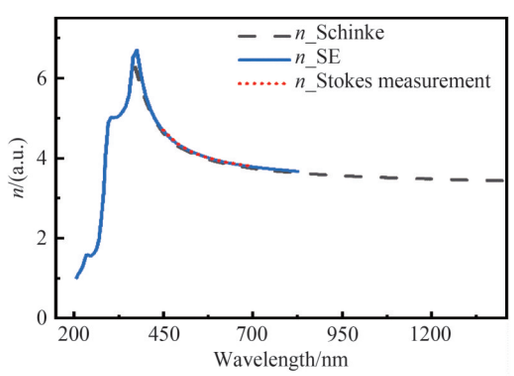

图 7 折射率实部对比结果

Fig. 7 Comparison result of real part of refractive index

过 50 倍物镜成像观测到彩色干涉条纹消失判定空气间隙可忽略(此时完成预压约为 2 GPa 左右)。图 8 为 2～9 GPa 下单晶硅椭偏测量结果。图 9 为与之对应的单晶硅的拉曼光谱的测量结果,可看到单晶硅的拉曼峰随着压力增大而红移,这与压力导致单晶硅晶格常数减小现象一致。

参考图 2(b)所示金刚石的反射光路,本文假设金刚石的上下两反射面的反射光束是完全分离的,因此,2.2 节中膜层理论所引入的椭偏参量值仅考虑金刚石的上表面或下表面的反射光。而实际测量过程中,由

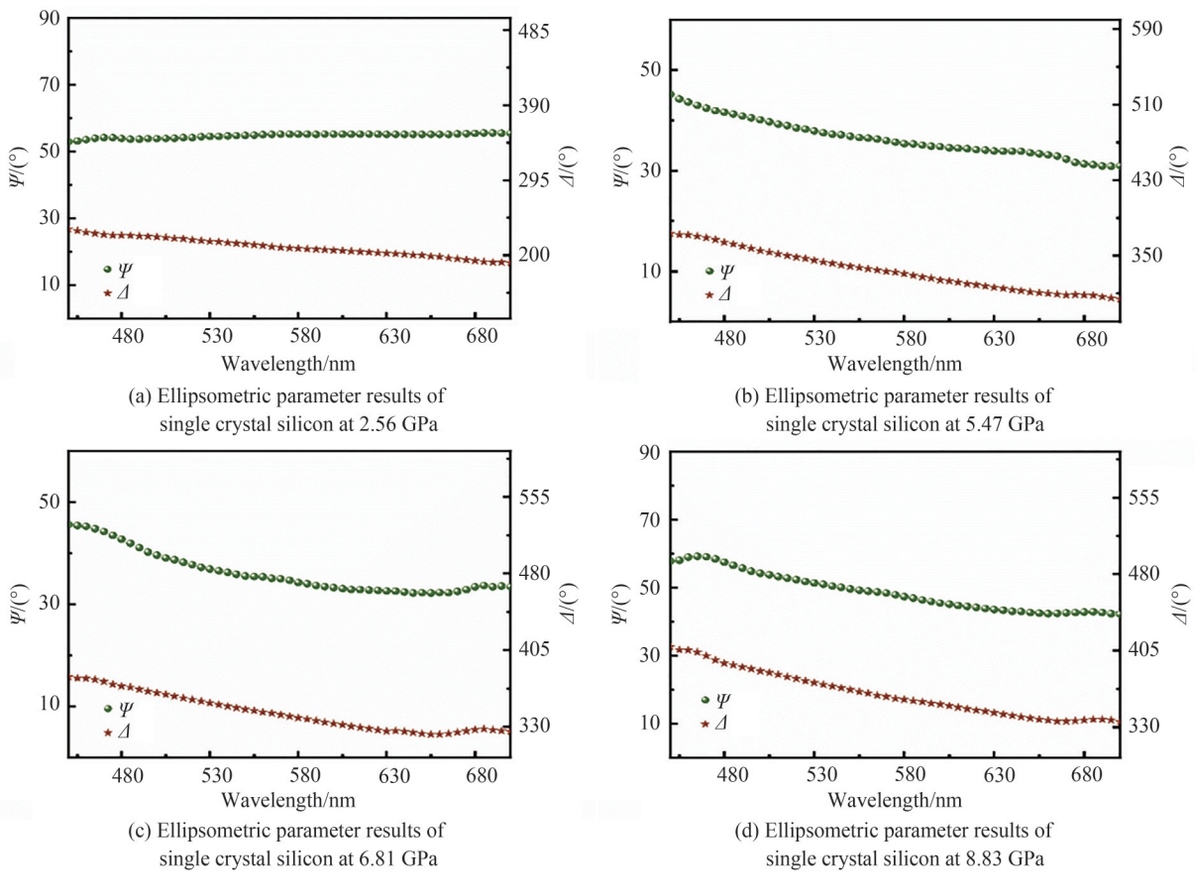

图8　不同压力下单晶硅椭偏参量结果图

Fig. 8　Ellipsometry parameter results of monocrystalline silicon under pressure loading

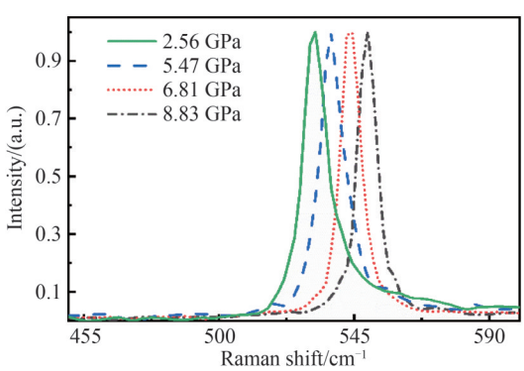

图9　压力加载下单晶硅拉曼测量结果

Fig. 9　Raman measurement results of monocrystalline silicon under pressure loading

于受DAC角度限制，通过狭缝进入偏振测量仪分别检测的两光束偏振信息中R_1的反射率高于R_2，因此，在进行R_2光束椭偏测量时，受到R_1的影响会引入误差。为此，在理论椭偏参量模型中引入校正参数模拟R_1的影响。校正后的理论椭偏参量ψ与实验结果对比如图10所示。校正后的椭偏参量与理论值基本相符。

在实验测量波段450～700 nm，采用柯西色散模型进行遗传算法拟合分析，分别得到不同压力下单晶硅折射率实部数据如图11所示。图中数据表明，随压力增大，单晶硅折射率整体呈现增大趋势。8.83 GPa折射率拟合结果表明压力增加会导致单晶硅的色散情况加剧。

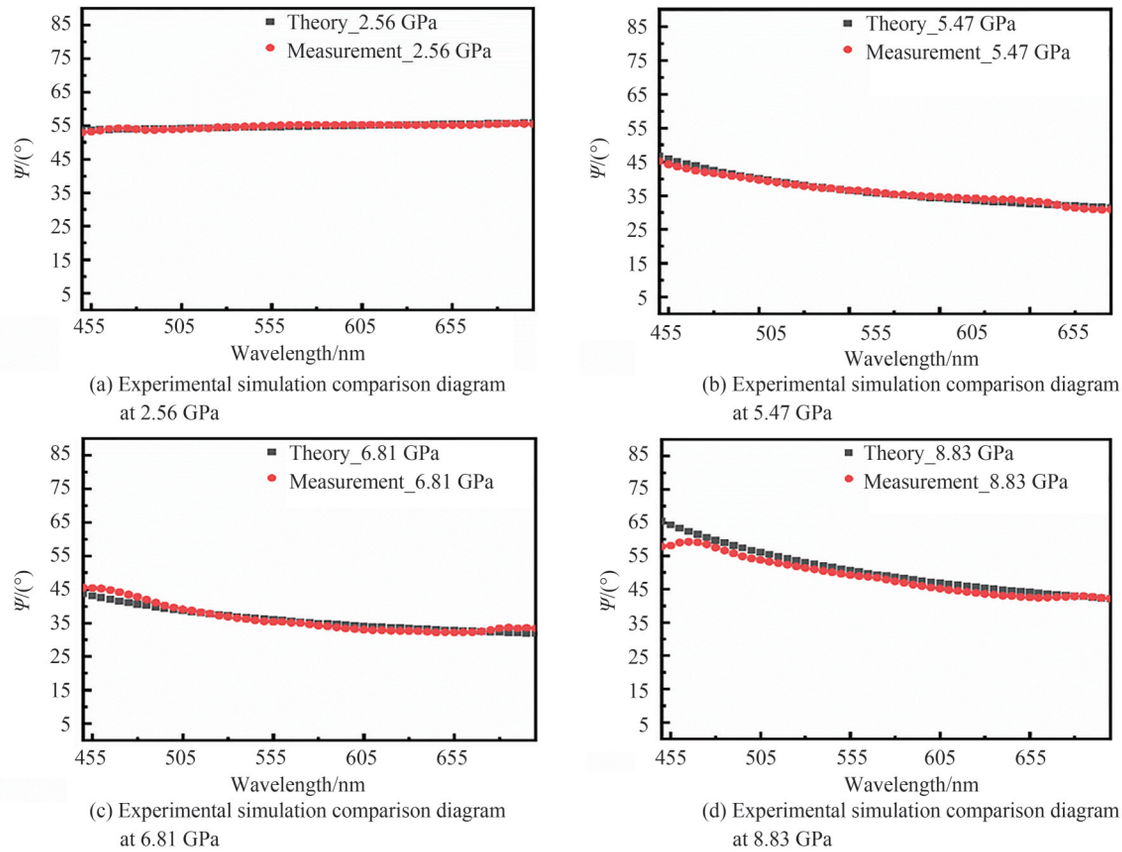

图 10 压力加载下单晶硅 ψ 值实验仿真对比

Fig. 10 Comparison of experimental simulation of monocrystalline silicon ψ value under pressure loading

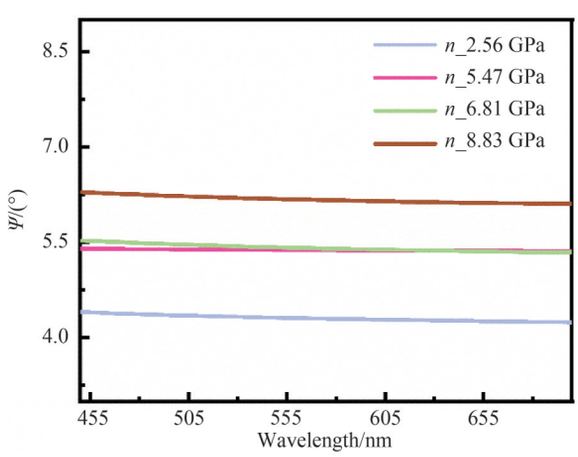

图 11 压力加载下单晶硅折射率结果

Fig. 11 Refractive index of monocrystalline silicon under pressure loading

3 结论

采用斯托克斯椭偏测量系统，针对DAC环境，实现了高压下小角度的椭偏测量。基于偏振测量的基本原理与高压加载技术，实验得到了2.56 GPa、5.47 GPa、6.81 GPa、8.83 GPa压力加载下单晶硅材料的椭偏参数信息，并采用遗传算法分析拟合各压强值对应下单晶硅符合柯西色散模型的折射率结果。实验结果表明，随着压力的增加，单晶硅的折射率呈现增大的趋势，并且色散加剧。受限于目前的DAC加工工艺，分别经过金刚石两反射面的光束存在一定程度相互影响，是本研究中测量误差的主要来源，有望通过金刚石界面加工工艺的改进，进一步减小这一误差，提升高压下光学常数测量的准确度。

参考文献

[1] LI Jianhua, CUI Yuanshun, CHEN Guibin. Structural phase transition, electronic structures and optical properties of GaN[J]. Acta Photonica Sinica, 2013, 42(2): 161-166.
李建华, 崔元顺, 陈贵宾. GaN结构相变、电子结构和光学性质[J]. 光子学报, 2013, 42(2): 161-166.

[2] FOATA P M, ROBERT G, NADAL M H, et al. First-principles study of the relations between the elastic constants, phonon dispersion curves, and melting temperatures of bcc Ta at pressures up to 1000GPa[J]. Physical Review B, 2007, 76(10): 104104.

[3] LEE P L, HUANG E, KUNG J. High-pressure Raman spectroscopy and X-ray diffraction study on scottyite, $BaCu_2Si_2O_7$[J]. Minerals, 2021, 11(6): 608.

[4] CHAO D, ZHUO J, CHAO F, et al. High-pressure Raman spectroscopy study of L-serine[J]. Spectroscopy and Spectral Anakysis, 2019, 39(3): 791-796.

[5] TANG H, YANG C, WANG G, et al. Raman spectroscopy for quantitative measurements of temperature and major species in high-pressure non-premixed $NH_3/H_2/N_2$ counterflow flames[J]. Combustion and Flame, 2022, 237: 111840.

[6] PAKORNCHOTE T, GEBALLE Z M, PINSOOK U, et al. Raman spectroscopy on hydrogenated graphene under high pressure[J]. Carbon, 2020, 156: 549-557.

[7] KUDRYAVTSEV D A, MFEDOTENKO T, KOEMETS E G, et al. Raman spectroscopy study on chemical transformations of propane at high temperatures and high pressures[J]. Scientific Reports, 2020, 10(1): 1483.

[8] MORIZET Y, JOLIVET V, TRCERA N, et al. Iodine local environment in high pressure borosilicate glasses: An X-ray photoelectron spectroscopy and X-ray absorption spectroscopy investigation[J]. Journal of Nuclear Materials, 2021, 553: 153050.

[9] JIA M, HU X, LIU Y, et al. X-ray diffraction and Raman spectra of merrillite at high pressures[J]. High Pressure Research, 2020, 40(3): 411-422.

[10] MAO W L, LIN Y, LIU Y, et al. Applications for nanoscale X-ray imaging at high pressure[J]. Engineering, 2019, 5(3): 479-489.

[11] GAIDA N A, GREAUX S, KONO Y, et al. Elasticity of nanocrystalline kyanite at high pressure and temperature from ultrasonic and synchrotron X-ray techniques[J]. Journal of the American Ceramic Society, 2021, 104(1): 635-644.

[12] RUNCORN S. Experiments on the displacement of the ultraviolet absorption edge of olivine at high pressures[J]. Journal of Applied Physics, 1956, 27(6): 598-602.

[13] YU J, TANG J, WANG X, et al. Synthesis of benzothiazole-azo disperse dyes for high resistance to alkaline treatments and peroxide bleaching[J]. Pigment & Resin Technology, 2022, 51(2): 186-193.

[14] PRUZAN P. Pressure-induced transformations of materials: light spectroscopy investigations[J]. International Journal of Materials and Product Technology, 2006, 26(3-4): 200-216.

[15] COBOS C J, HINTZER K, SOLTER L, et al. High-temperature fluorocarbon chemistry revisited[J]. The Journal of Physical Chemistry A, 2021, 125(25): 5626-5632.

[16] BAKSHI L, ELIEZER S, HENIS Z, et al. Equations of State and the ellipsometry diagnostics[J]. Laser and Particle Beams, 2009, 27(1): 79-84.

[17] NISSIM N, ELIEZER S, BAKSHI L, et al. High pressure ellipsometry: a novel method for measuring the optical properties and electronic structure of materials in diamond anvil cells[J]. Review of Scientific Instruments, 2011, 82(3): 033905.

[18] WANG Yifan. Spectroscopic ellipsometry under high pressure loaded by diamond anvil[D]. Wuhan: Huazhong University of Science Technology, 2021.
王一帆. 金刚石压砧高压加载下光谱椭偏测量方法研究[D]. 武汉: 华中科技大学, 2021.

[19] ZHANG Dongqing, WANG Xiangchao, SHI Weijie. In situ measurement technology for surface roughness of Stepper silicon wafer[J]. Acta Photonica Sinica, 2006, 35(12): 1976-1979.
张冬青, 王向朝, 施伟杰. 光刻机硅片表面不平度原位检测技术[J]. 光子学报, 2006, 35(12): 1976-1979.

[20] DING Yueke, HUANG Shihua. Study on passivation of monocrystalline silicon by tandem hydrogenated amorphous silicon film[J]. Acta Photonica Sinica, 2021, 50(3): 0331001.
丁月珂, 黄仕华. 氢化非晶硅叠层薄膜对单晶硅表面钝化研究[J]. 光子学报, 2021, 50(3): 0331001.

[21] HANFLAND M, SYASSEN K. A Raman study of diamond anvils under stress[J]. Journal of Applied Physics, 1985, 57(8): 2752-2756.

[22] SCHINKE C. Uncertainty of the coefficient of band-to-band absorption of crystalline silicon[J]. AIP Advances, 2015, 5(6): 67168-67168.

Ellipsometric Measurement of the Refractive Index of Monocrystalline Silicon in a Diamond Anvil Cell

BAO Xiaoyan, DENG Shuo, LV Haifei, LI Min
(*School of Science, Wuhan University of Technology, Wuhan* 430070, *China*)

Abstract: High-pressure physics has advanced significantly since its inception, initially being used to study the structure of materials within the Earth. Today, it has applications in various scientific fields, such as chemistry, physics, biology, materials science, and pharmacy. Through the development of advanced instruments and software, high pressure research has become more precise, comprehensive, and complex.

Compared to the momentary pressure changes brought by dynamic high pressure shock, static high pressure loading has the advantages of safety, cleanliness, and low response time requirements for detection equipment. In the late 1950 s, high pressure science entered the era of Diamond Anvil Cells (DACs). In the following decades, DAC technology has been continuously improved, including increasing the chamfer of the opposing anvils to further increase pressure, improving the metal gasket materials, and introducing pressure transmission media. These improvements have increased pressure while solving problems such as pressure gradients and sample leakage. The continuous improvement and development of these technologies have not only expanded the upper limit of pressure that experimental techniques can achieve but also greatly promoted the development of high-pressure science. Diamond anvil cells, due to their unique structure, can generate high pressure on a small area and are widely used in studying material properties under high pressure. In-situ optical radiation measurement techniques in diamond anvil cells include high-pressure Raman spectroscopy, high-pressure synchrotron X-ray radiation, photoluminescence spectroscopy, ultraviolet-visible absorption spectroscopy, and infrared spectroscopy. However, most existing optical detection methods for diamond anvils require expensive large-scale detection equipment, such as synchrotron radiation sources. Furthermore, these methods are often focused on the absorption spectrum or photoluminescence properties of the materials themselves without directly measuring the material′s optical constants.

This study aims to obtain refractive index data for materials inside the diamond anvil cell under different pressures through in-situ Small-Angle Ellipsometry (SAE). Ellipsometry is a non-contact, non-destructive optical detection method that modulates the polarization state of the light beam when reflected or transmitted on the sample surface. By detecting the polarization state changes of the incident light beam before and after reflecting from the sample, the proposed SAE obtains information such as the optical constants of the thin film to be measured.

To achieve this goal, the study designs an in-situ small-angle ellipsometry system to satisfy the special measurement conditions of limited incident angle, long working distance, and miniature sample size under high pressure. The system achieves small-angle ellipsometry in the 450～700 nm spectral range. It monitors the changes in the Stokes vector of the incident light beam before and after reflection from the sample inside the diamond anvil cell. It obtains the reflectance ellipsometric parameters ψ and Δ for isotropic samples under pressure loading.

However, due to the actual multiple-layer film transmission inside the diamond anvil cell, the iterative analysis formula for complex refractive index calculation is too complicated the transfer matrix method is employed for calculation. The polarization state of the light beam is described by the Jones vector. After reflection, transmission, and interlayer transmission, the polarization state of the light beam changes and can be described by a 2×2 Jones matrix. Theoretical ellipsometric parameters are then extracted based on the matrix calculation results. The study uses numerical simulation software to set a fitting evaluation function and obtains the real part of the refractive index information for the sample under test. The study measures four sets of information for real-time loaded diamonds under pressure and calibrates the loading pressure value using the diamond Raman peak.

Finally, the real part of the refractive index information for single crystal silicon under a pressure range of 2～9 GPa is obtained. The study also performs in-situ Raman detection on the same sample. The experimental results show that the refractive index of single crystal silicon increases with increasing pressure in the pressure range of 2.56 GPa to 8.81 GPa, which is consistent with the redshift trend

observed in the Raman spectra.

The development of this small-angle in-situ ellipsometry system provides a useful supplement for the optical constants and in-situ measurement of materials under high pressure, which is critical for exploring the optical properties of other thin films on silicon substrates under high pressure and for understanding the interplay between pressure and optical properties. Moreover, the small-angle in-situ ellipsometry system designed in this study can be used for in-situ measurement of the optical properties of other materials under high pressure, expanding the scope of high-pressure research and promoting the development of related fields.

In summary, high-pressure physics plays a crucial role in various fields, and the study of materials under high pressure provides important insights into their properties and behavior. The use of diamond anvil cells and in-situ optical radiation measurement techniques have significantly advanced high-pressure research, but there is still a need for new, more efficient, and cost-effective methods. The small-angle in-situ ellipsometry system developed in this study provides a promising new approach for in-situ measurements of material properties under high pressure. By obtaining refractive index data for single crystal silicon inside the diamond anvil cell, this system can provide a new perspective and help researchers gain a better understanding of how pressure affects the optical properties of materials, which can have significant implications for a wide range of applications.

Key words: High pressure; Ellipsometry; Optical model; Refractive index; Monocrystalline silicon
OCIS Codes: 240.0310; 240.2130; 120.4530

Foundation item: National Natural Science Foundation of China (Nos. 11974266, 62075174)